Chair of Structural Analysis
Technical University of Munich
Andreas Apostolatos

Multipatch Isogeometric Analysis for Lightweight Structures with Application to Partitioned Fluid-Structure Interaction

Non-Uniform Rational B-Spline basis functions

Classical Finite Element Analysis (FEA) uses typically C^0-continuous basis functions across the elements which also attain low polynomial order for numerically confronting Boundary Value Problems (BVPs). On the other hand, Isogeometric Analysis (IGA), firstly proposed in [1], makes use of high order basis functions the so-called Non-Uniform Rational B-Spline (NURBS) which in addition attain higher than C^0-continuity across the elements.

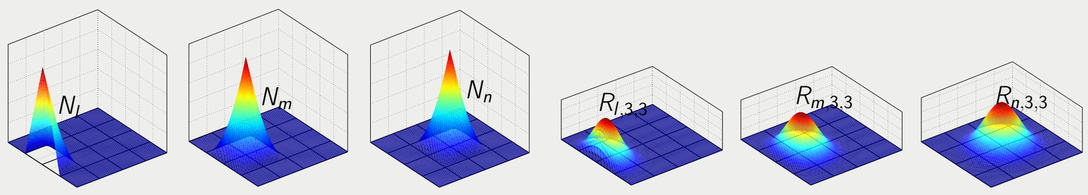

(a) Low order FEA basis functions (b) High order NURBS basis functions

Figure: Piece-wise polynomial basis functions.

The NURBS basis functions can be iteratively computed in 1D as:

$$N_{i,0}(\xi) = \begin{cases} 1 & \text{if } \xi \in [\xi_i, \xi_{i+1}[\\ 0 & \text{elsewhere} \end{cases}, \quad \text{and } N_{i,p}(\xi) = \frac{\xi - \xi_i}{\xi_{i+p} - \xi_i} N_{i,p-1}(\xi) + \frac{\xi_{i+p+1} - \xi}{\xi_{i+p+1} - \xi_{i+1}} N_{i+1,p-1}(\xi)$$

$$R_{i,p}(\xi) = \frac{N_{i,p}(\xi)}{\sum_{j=1}^{n} N_{j,p}(\xi)\, w_j} .$$

The main benefits in using the above basis for the analysis consist in the exact geometry representation, adjustable smoothness across the knot spans (elements) and high order field approximation.

Multipatch isogeometric analysis

Isogeometric analysis is extended to account for multiple domains, see [2, 3]. This extension is necessary because the vast majority of the CAD models comprise multipatch geometries. Correspondingly, the decomposed Kirchhoff-Love shell BVP reads,

$$\begin{aligned}
n^{\alpha\beta}\big|_\alpha - q^\alpha B_\alpha^{\ \beta} + b^\beta &= 0 , \quad \text{in } \Omega \setminus \Gamma_c , \\
n^{\alpha\beta} B_{\alpha\beta} + q^\alpha\big|_\alpha + b^3 &= 0 , \quad \text{in } \Omega \setminus \Gamma_c , \\
m^{\alpha\beta}\big|_\alpha - q^\beta &= 0 , \quad \text{in } \Omega \setminus \Gamma_c , \\
\mathbf{d} &= 0 , \quad \text{on } \subset \Gamma_d , \\
\boldsymbol{\omega} &= 0 , \quad \text{on } \subset \Gamma_d , \\
\mathbf{n}^\alpha u_\alpha &= \mathbf{p} , \quad \text{on } \subset \Gamma_n \\
\mathbf{m}^\alpha u_\alpha &= \mathbf{r} , \quad \text{on } \subset \Gamma_n \\
\mathbf{d}^{(i)} - \mathbf{d}^{(j)} &= 0 , \quad \text{on } \Gamma_c^{(i,j)}\ \forall i,j = 1,\dots,n , \\
\boldsymbol{\omega}^{(i)} + \boldsymbol{\omega}^{(j)} &= 0 , \quad \text{on } \Gamma_c^{(i,j)}\ \forall i,j = 1,\dots,n ,
\end{aligned}$$

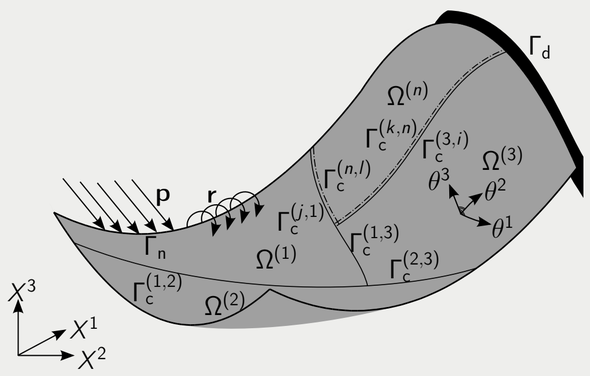

Figure: Problem placement for the Kirchhoff-Love shell in multiple domains

Three methods are employed for the establishment of a weak form to the coupled system. The first one is the *Penalty*, for which the Newton-Raphson subproblem in the i-th iteration writes,

$$\begin{bmatrix} \mathbf{K}_{\mathrm{T},\hat{i}}^{(1)} + \mathbf{K}_{\mathrm{p}}^{(1)} & \cdots & \mathbf{C}_{\mathrm{p}}^{(1,n)} \\ \vdots & \ddots & \vdots \\ \mathbf{C}_{\mathrm{p}}^{(n,1)} & \cdots & \mathbf{K}_{\mathrm{T},\hat{i}}^{(n)} + \mathbf{K}_{\mathrm{p}}^{(n)} \end{bmatrix} \begin{bmatrix} \delta\hat{\mathbf{d}}_{\hat{i}}^{(1)} \\ \vdots \\ \delta\hat{\mathbf{d}}_{\hat{i}}^{(n)} \end{bmatrix} = - \begin{bmatrix} \mathbf{R}_{\hat{i}}^{(1)} \\ \vdots \\ \mathbf{R}_{\hat{i}}^{(n)} \end{bmatrix} - \begin{bmatrix} \mathbf{K}_{\mathrm{p}}^{(1)} & \cdots & \mathbf{C}_{\mathrm{p}}^{(1,n)} \\ \vdots & \vdots & \ddots \\ \mathbf{C}_{\mathrm{p}}^{(n,1)} & \cdots & \mathbf{K}_{\mathrm{p}}^{(i)} \end{bmatrix} \begin{bmatrix} \hat{\mathbf{d}}_{\hat{i}}^{(1)} \\ \vdots \\ \hat{\mathbf{d}}_{\hat{i}}^{(n)} \end{bmatrix} .$$

The second one is the *Lagrange Multipliers* method, which introduces two additional Lagrange Multipliers fields, one for each interface condition. The corresponding equation system for the Newton-Raphson subproblem writes,

$$\begin{bmatrix} \mathbf{K}_{\mathrm{T},\hat{i}}^{(1)} & \cdots & \mathbf{0} & \boldsymbol{\Lambda}^{(1)} & \mathbf{Z}^{(1)} \\ \vdots & \ddots & \vdots & \vdots & \vdots \\ \mathbf{0} & \cdots & \mathbf{K}_{\mathrm{T},\hat{i}}^{(n)} & \boldsymbol{\Lambda}^{(n)} & \mathbf{Z}^{(n)} \\ \boldsymbol{\Lambda}^{(1)\mathrm{T}} & \cdots & \boldsymbol{\Lambda}^{(n)\mathrm{T}} & \mathbf{0} & \mathbf{0} \\ \mathbf{Z}^{(1)\mathrm{T}} & \cdots & \mathbf{Z}^{(n)\mathrm{T}} & \mathbf{0} & \mathbf{0} \end{bmatrix} \begin{bmatrix} \delta\hat{\mathbf{d}}_{\hat{i}}^{(1)} \\ \vdots \\ \delta\hat{\mathbf{d}}_{\hat{i}}^{(n)} \\ \delta\hat{\boldsymbol{\lambda}}_{\hat{i}} \\ \delta\hat{\boldsymbol{\zeta}}_{\hat{i}} \end{bmatrix} = - \begin{bmatrix} \mathbf{R}_{\hat{i}}^{(1)} \\ \vdots \\ \mathbf{R}_{\hat{i}}^{(n)} \\ \mathbf{0} \\ \mathbf{0} \end{bmatrix} - \begin{bmatrix} \mathbf{0} & \cdots & \mathbf{0} & \boldsymbol{\Lambda}^{(1)} & \mathbf{Z}^{(1)} \\ \vdots & \ddots & \vdots & \vdots & \vdots \\ \mathbf{0} & \cdots & \mathbf{0} & \boldsymbol{\Lambda}^{(n)} & \mathbf{Z}^{(n)} \\ \boldsymbol{\Lambda}^{(1)\mathrm{T}} & \cdots & \boldsymbol{\Lambda}^{(n)\mathrm{T}} & \mathbf{0} & \mathbf{0} \\ \mathbf{Z}^{(1)\mathrm{T}} & \cdots & \mathbf{Z}^{(n)\mathrm{T}} & \mathbf{0} & \mathbf{0} \end{bmatrix} \begin{bmatrix} \hat{\mathbf{d}}^{(1)} \\ \vdots \\ \hat{\mathbf{d}}^{(n)} \\ \hat{\boldsymbol{\lambda}}_{\hat{i}} \\ \hat{\boldsymbol{\zeta}}_{\hat{i}} \end{bmatrix} .$$

As last, the *augmented Lagrange Multipliers* method is elaborated. This method is essentially the Lagrange Multipliers method enhanced with the penalty terms.

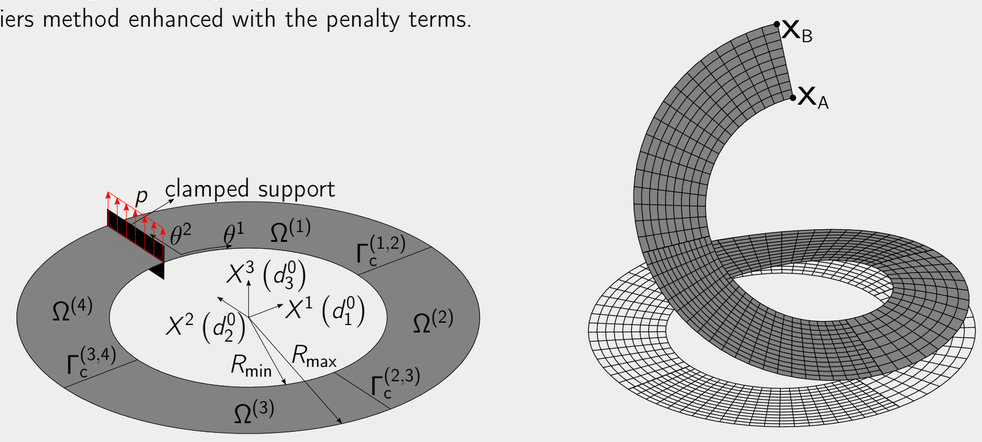

(a) Problem placement. (b) Ultimate deformation.

Figure: Slit annular plate: Ultimate deformation and moment field $\overline{m}^{22}$.

A comparison of the methods is demonstrated with a nonlinear benchmark problem proposed in [4] and the corresponding results are given. Emphasis must be given to the smoothness that the methods deliver across the patch interfaces. All methods produce almost the same results, which verifies the consistency of the extended variational formulations. In regard to the Penalty method, the choice of the penalty factors must be careful so that they are large enough to satisfy the interface conditions but not deteriorate the condition number of the equation system. In relation to the Lagrange Multipliers method, attention has to be taken in the choice of the discretization for the Lagrange Multipliers fields, because improper choice can lead to indeterminate systems.

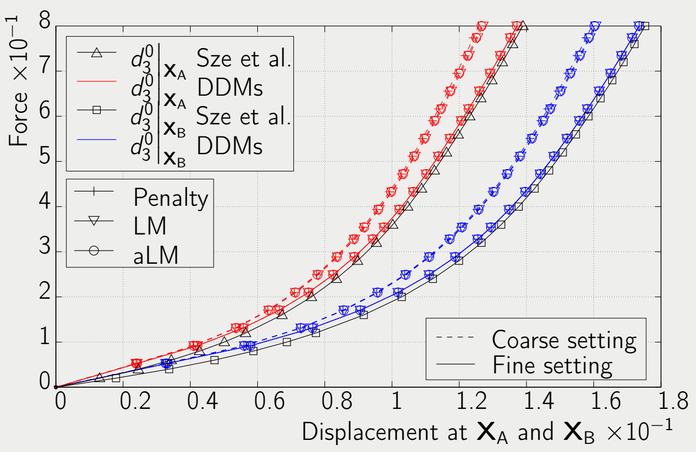

Figure: Load displacement curves.

Non-matching grid data transfer between classical finite element and isogeometric grids

The method of choice within this study is the so-called *Mortar* method, which is based on the minimization of the gap function $\mathbf{d}_{\mathrm{h}}^{(\mathrm{S})} - \mathbf{d}_{\mathrm{h}}^{(\mathrm{F})}$ between the structural and the fluid mesh displacement fields in the $L^2(\Gamma_{\mathrm{FSI}})$ space, namely:

$$\int_{\Gamma_{\mathrm{FSI}}} \left(\mathbf{d}_{\mathrm{h}}^{(\mathrm{S})} - \mathbf{d}_{\mathrm{h}}^{(\mathrm{F})} \right) \cdot \boldsymbol{\mu}\, \mathrm{d}\Gamma = 0 \qquad \forall \boldsymbol{\mu} \in \left(L^2(\Gamma_{\mathrm{FSI}}) \right)^3 .$$

In its discrete form, the mortar method writes:

$$\hat{\mathbf{d}}^{(\mathrm{F})} = \left(\mathbf{C}^{(\mathrm{F})} \right)^{-1} \mathbf{C}^{(\mathrm{S})} \hat{\mathbf{d}}^{(\mathrm{S})} ,$$

where the hat in the above vectors indicates that they contain the respective degrees of freedom. The coupling matrices are given by:

$$\mathbf{C}^{(\mathrm{S})} = \int_{\Gamma_{\mathrm{FSI}}} (\mathbf{N}^{\mu})^{\mathrm{T}} \mathbf{R}\, \mathrm{d}\Gamma \quad \text{and} \quad \mathbf{C}^{(\mathrm{F})} = \int_{\Gamma_{\mathrm{FSI}}} (\mathbf{N}^{\mu})^{\mathrm{T}} \mathbf{N}^{(\mathrm{F})}\, \mathrm{d}\Gamma ,$$

$\mathbf{N}^{\mu}$, $\mathbf{R}$ and $\mathbf{N}^{(\mathrm{F})}$ being the basis function matrices for the Lagrange Multipliers field $\boldsymbol{\mu}$, the structural and the fluid mesh displacement field across the interface, respectively.

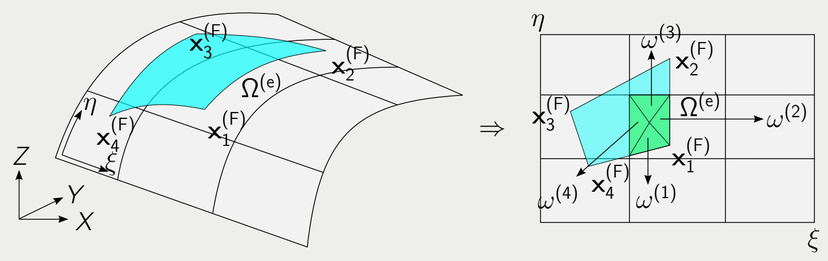

Figure: Clipping of the projected fluid elements

Figure: Projection phase

In the mortar method the choice $\mathbf{N}^{\mu} = \mathbf{N}^{(\mathrm{F})}$ is made, so that the transformation matrix $\mathbf{T} = \left(\mathbf{C}^{(\mathrm{F})} \right)^{-1} \mathbf{C}^{(\mathrm{S})}$ is symmetric, positive definite and diagonally dominant. A unique interface must be identified so that the above integrals can be evaluated. Especially in case of data exchange between B-Spline surfaces and Finite Volume elements, the bases are always non-conforming across the interface. For this reason each fluid node is orthogonally projected onto the B-Spline surface. Then, the integration is performed at the sub-element level. If the discrete virtual work over the interface is to be preserved, namely $\delta\mathcal{W}^{(\mathrm{S})} = \delta\mathcal{W}^{(\mathrm{F})}$ on Γ_{FSI}, then matrix $\mathbf{T}^{\mathrm{T}}$ can be used for the force transfer.

Flow over semispherical pressurized membrane

A pressurized semispherical membrane is employed in a fluid-structure interaction environment for the comparison of the results obtained by the classical FEA and IGA for the discretization of the structural field. The membrane has Young's modulus, poisson's ratio and structural density equal to 10^2 KN/m^2, 0.3 and 1700 Kg/m^3, respectively, whereas it's radius and it's thickness are equal to 50 cm and 1 mm, respectively. In addition, the membrane is subject to internal pressure equal to 10 N/m^2 so that it stays in semispherical shape when no other loading conditions are prescribed. For the structural problem both classical FEA and IGA are employed using the software Carat++, Chair of Structural Analysis, Prof. Dr.-Ing. Kai-Uwe Bletzinger. The fluid is assumed to be the air, modelled as a Newtonian incompressible fluid with density and dynamic viscosity equal to 1.225 Kg/m^3 and 18.27$\times$ 10^{-6} Kg/m/s, respectively. Open∇FOAM, see `http://www.openfoam.org/`, is an open source software which was used in this study for the fluid problem. On the other hand, EMPIRE, see `http://empire.st.bv.tum.de/` is used for the communication of the fields across their interfaces.

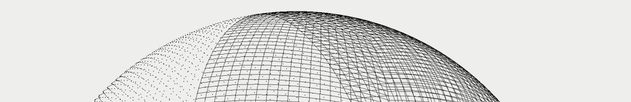

Figure: Problem setting for the pressurized semisphere in flow.

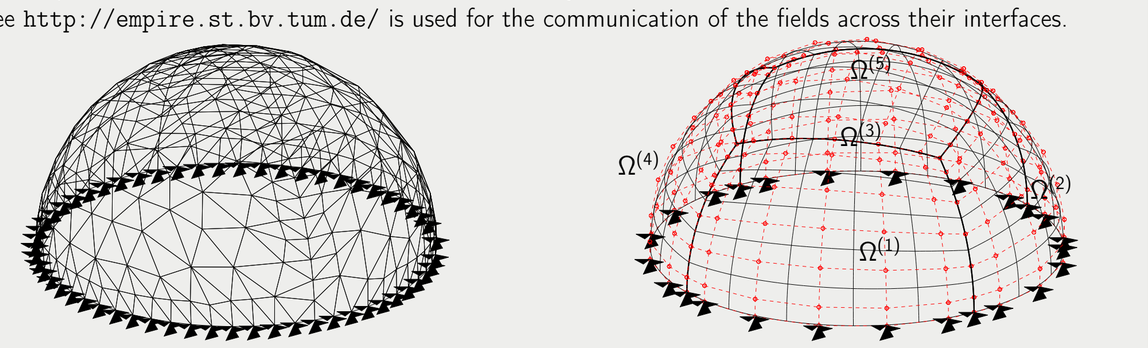

(a) The membrane discretized with triangular elements (b) The membrane modelled with 5 patches

Figure: Modelling and discretization of the semispherical membrane.

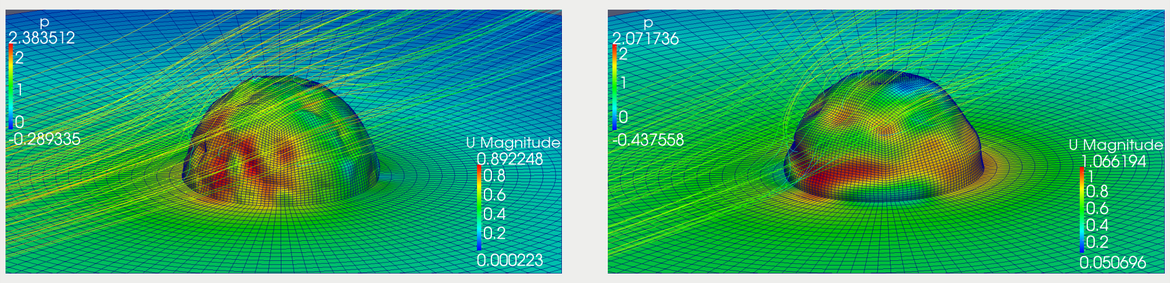

(a) Classical Finite Element Membrane. (b) Isogeometric Membrane.

Figure: Deformation of the membrane structure at $t = 0.4$ s.

References

[1] J.A. Cottrell, T.J.R. Hughes, and Y. Bazilevs. *Isogeometric Analysis: Toward Integration of CAD and FEA*. Wiley, 2009.

[2] A. Apostolatos, R. Schmidt, R. Wüchner, and K.-U. Bletzinger. "A Nitsche-type formulation and comparison of the most common domain decomposition methods in isogeometric analysis". In: *International Journal for Numerical Methods in Engineering* 97 (2014), pp. 473–504. ISSN: 1097-0207.

[3] M. Breitenberger, A. Apostolatos, B. Philipp, R. Wüchner, and K.-U. Bletzinger. "Analysis in computer aided design: Nonlinear isogeometric b-rep analysis of shell structures". In: *Computer Methods in Applied Mechanics and Engineering* 284 (2015), pp. 401 –457. ISSN: 0045-7825.

[4] K.Y. Sze, X.H. Liu, and S.H. Lo. "Popular benchmark problems for geometric nonlinear analysis of shells". In: *Finite Elements in Analysis and Design* 40.11 (2004), pp. 1551–1569. ISSN: 0168-874X.

andreas.apostolatos@tum.de http://empire.st.bv.tum.de, Lehrstuhl für Statik Prof. Dr.-Ing. K.-U. Bletzinger http://www.st.bgu.tum.de